31st Annual International Conference of the IEEE EMBS
Minneapolis, Minnesota, USA, September 2-6, 2009

Robot-Assisted Light Dose Evaluation for Endoscopically Guided Photodynamic Therapy: A Preliminary Study

Dongwen Zhang, Lei Wang, Jia Gu, Zhen Zheng

Abstract—**Conventional endoscope-guided photodynamic therapy (PDT) suffers mostly from motion artifacts, therefore expert hand-eye coordination was always needed during manual operations. In this paper we introduced a visual servo scheme to handle the tracking problem between the focused area and the targeted lesions. The scheme is consisted of real-time feature matching, relative motion cancellation and real-time light dose surveillance. Experiments were carried out both on simulated data and a silicon phantom. It indicats that this scheme outperforms the conventional scheme in terms of reduction in operation time and exposure to healthy tissue.**

I. Introduction

SINCE Lipson and Baldes reported the phototoxicity of photosensitizer in the 1960s, photodynamic therapy (PDT) became a powerful alternative after chemotherapy and radiotherapy for tumor therapy. PDT has been used for localized superficial or endoluminal malignant, etc. Furthermore its application has also been expanded to solid tumors and metastases recently [1]. The minimally invasive nature of PDT also offers great promise in some non-malignant conditions in dermatology, ophthalmology and cardiology.

Endoscopically guided PDT is one of the most frequently performed operations for upper gastrointestinal tumors because of its relative convenience in operating field localization and hand-eye monitoring. Treatment usually lasts a few minutes to a few tens of minutes. A simple light dose controlling strategy is that timer-controlled switch turns off when operating time exceeds a designated value. Although photosensitizers are selectively retained in cancer cells, they can also make healthy cells around sensitive to light. Coupled with physiological movement of digestive tract, the region of interest (ROI) moves co-operatively back and forth from the focused area. Photochemical reaction occurs when nearby healthy tissue is exposed to irradiation, severity of damage depends on equivalent exposure and movement range. Lacking in-situ surveillance, conventional PDT can not provide valid optical dose controlling and practical risk hedging strategy.

Physiological motion compensation by robot is a very promising approach for assisting surgeon in difficult operations. Sharma et al. and Schweikard et al. studied the compensation of the breathing motion in order to reduce the applied radiation dose to irradiated tumors[2],[3], Özkan Bebek presented an active relative motion cancellation (ARMC) frame to stabilize dynamically the heart employing biological signals in off-pump coronary artery bypass graft (CABG) surgery [4]. Quite different from the situations above, in which absolute movement can be measured by the positioning system located outside the body, endoscopically guided PDT could only monitor relative movement of ROI without any auxiliary setup. The main difference lies in the difficulty of obtaining a kinematics model for these flexible systems.

Manuscript received April 23, 2009. This work was supported by Guangdong Natural Science Foundation of China(Grant NO. 8178922035) and Public S&T Project of Shenzhen(Grant NO.SY200806300230A).

The authors are with Research Center for Medical Robotics and MIS Device, Shenzhen Institute of Advanced Technology, Shenzhen, China (e-mail: wang.lei@siat.ac.cn)

II. Method

The surgeon faces numerous challenges when manually controlling the navigation wheels to rotate the tip along two orthogonal directions and pulling the endoscope forward/backward to track target site during PDT operations.

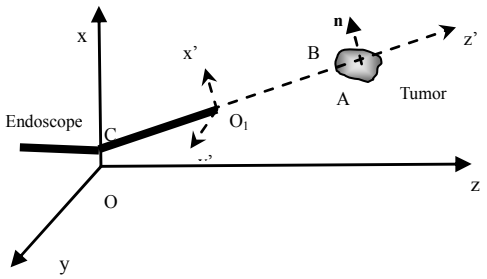

Fig. 1. Overview of coordinates correspondence

The instantaneous motion of the camera $\mathbf{A} = [x_A(t), y_A(t), z_A(t)]^T$ was primarily a translation in the image plane, which depends on the nearest point tangent to the wall of digestive tract. We locate the shaft part of endoscope parallel to primary axis z, an overview of coordinates correspondence of each component can be seen in Fig 1. To compensate relative motion between focused optical center $\mathbf{C} = [x_C(t), y_C(t), z_C(t)]^T$ and tumor center $\mathbf{B}$, a visual servo scheme was put forward to handle this tracking problem in association with relevant features matching and light dose estimation.

A. Physiological Motion Analysis

Patients need to fast for 8 to 10 hours before endoscope-guided PDT therapy, The MMC (Migrating Motor Complex) originates in the stomach and moves to ileocecal valve roughly every 75-90 minutes during the interdigestive phase [5]. Coupled with physiological movements, maladjustment of the endoscope appears more significantly in

the stomach than narrow esophagus and duodenum. To represent these relative movements, we assume the synchronous component $\Pi(t)$ induced by breathing and heartbeat can be approximated as quasiperiodic and low frequency, while the asynchronous component $\Gamma(t)$ is something different. An overall effect can be formulated to:
Synchronous component:

$$\Pi(t) = B\sin(\omega_B t + \varphi_B) + H\sin(\omega_H t + \varphi_H) \quad (1)$$

Asynchronous component:

$$\Gamma(t) = \sum M \exp[-\frac{(t_i - t_M)^2}{2\sigma_M^2}] \quad (2)$$

To simulate the real-world case, the data were mixed with additive Gaussian noise $e_m(t)$. For target tracking, we pay more attention to ROI translation rather than tissue deformation. In computer vision, advanced identification and tracking of surface features is a well researched topic, a large number of robust feature descriptors have been proposed. More impressive progress of soft tissue deformation tracking can be seen in [6], [7].

B. Depth and Valid Light Dose Estimation

Reconstruction of 3D positions from 2D image plane is ill-posed without any prior information. Fortunately, relative depth d of tumor away from camera plane estimated by projected spot will get the solution much easier. As depicted in Fig 2, relative depth d and incident angle θ can be calculated geometrically from long axis l_2, short axis l_1 and scattering angle φ.

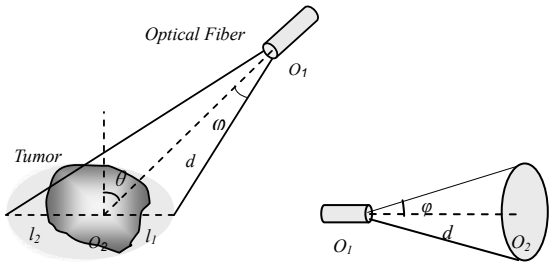

Fig. 2. Light dose evaluation frame

$$d = \frac{l_1 l_2}{\sin\varphi\sqrt{l_1^2 + l_2^2}} \quad (3)$$

$$\theta = \arctan(\frac{l_2}{l_1}) - \varphi \quad (4)$$

Based on fully understanding the luminous condition of target lesion, clinician customizes the light dose W. The optical power density I_i of focused area S_{O2} is inversely proportional to square of irradiation distance d along optical axis O_1O_2, and assumed to be uniform on focused plane.

$$I_i = \frac{P}{\pi d^2 \sin^2\varphi} \quad (5)$$

Valid optical power P_i is given by product of I_i and target site area S_{O2} exposed to irradiation, whereas the residual light dose P_r is estimated by (7)

$$P_i = S_{O2} I_i \quad (6)$$

$$P_r = W - \sum P_i t_i S_{O2} \quad (7)$$

Irradiation depth d should vary adaptively to get focused area over target site with minimal exposure to healthy structure.

$$\Delta d = \Delta R \csc\varphi \quad (8)$$

ΔR refers to variance in radius of the minimum circumcircle that enclosing the ROI.

C. Relative Motion Cancellation

In order to supply a robotic assistance to surgeons during flexible endoscopically guided PDT interventions, an automated relative motion compensation scheme is proposed. Ignoring tissue deformation, the target site is simplified to a facet with norm $\mathbf{n} = [n_x, n_y, n_z]^T$. We denote $\mathbf{Q} = [x, y, z]^T$ the relative motion between focused center $\mathbf{C}$ and target lesion $\mathbf{B}$, which is constrained in (10)

$$\mathbf{Q} = \mathbf{B} - \mathbf{C} \quad (9)$$

$$\mathbf{n}_C^T \mathbf{P}\mathbf{Q} = 0 \quad (10)$$

The direction number of AC is $\mathbf{n}_C = [\cos\alpha, \cos\beta, \cos\gamma]^T$, projection matrix $\mathbf{P}$ can be determined by incident angle and rotation of projected spot in image plane. Visual motion $\mathbf{F} = [u, v]^T$ in image plane is related to the joint motion $\mathbf{Q}$ by the interaction matrix denoted $\mathbf{J}$, which can be decomposed the following way: $\mathbf{J} = \mathbf{J}c\mathbf{J}q$. Perspective projection model is employed to describe the affine transform matrix $\mathbf{J}c$, $\mathbf{J}q$ donates the rotation frame of camera coordinates with respect to world coordinates.

$$\mathbf{F} = \mathbf{J}c\mathbf{J}q\mathbf{P}\mathbf{Q} \quad (11)$$

$$\mathbf{J}c = \begin{bmatrix} \frac{s}{d} & 0 & 0 \\ 0 & \frac{s}{d} & 0 \end{bmatrix} \quad (12)$$

Visual link between joint increments $\mathbf{\Lambda} = [\Delta\alpha, \Delta\beta]^T$ in two orthogonal directions and joint motion $\mathbf{Q}$ is built in (13)

$$\mathbf{\Lambda} = \mathbf{J}s\mathbf{P}\mathbf{Q} \quad (13)$$

If deviations of relative motion far less than the distance between inflexion point of endoscope and target site, $\mathbf{J}s$ can be simplified to

$$\mathbf{J}s = \begin{bmatrix} \frac{\sin\alpha}{L+d} & 0 & 0 \\ 0 & \frac{\sin\beta}{L+d} & 0 \end{bmatrix} \quad (14)$$

L refers to the length of bending part. Furthermore, increments $\mathbf{\Lambda}$ can be updated uniquely employing feature motions with integration of (10),(11),(13)

$$\mathbf{\Lambda} = \mathbf{J}s \begin{bmatrix} \mathbf{J}c\mathbf{J}q \\ \mathbf{n}_C^T \end{bmatrix}^{\dagger} \begin{bmatrix} \mathbf{F} \\ 0 \end{bmatrix} \tag{15}$$

We conclude the whole workflow as follows:

(1) Initial estimations for $[\alpha(0), \beta(0), d(0)]$;

(2) Update visual relative motion $[u, v]^T$, residual light dose P_r and depth d;

(3) One-step forecasting of $\mathbf{Q}(n+1)$;

(4) Update laser beam orientation and irradiation depth $[\Delta\alpha, \Delta\beta, \Delta d]^T$;

Go to step 2 until the residual light dose approaches to zero.

III. EXPERIMENTS

Our experiment involves two steps: relative motion cancellation algorithm tested on simulated data; supervised PDT efficiency evaluated on a movable silicon phantom.

A. Simulated Experiment

To represent the typical movement in quiescent and active phase, we put synchronous and asynchronous component distinctively to inflexion point C and tumor B. The waveforms were depicted in Fig 3.

1D relative motion tracking: synchronous component and asynchronous part moves along axis x independently;

$$[x_B(t), y_B(t), z_B(t)]^T = [C_1\Pi(t) + \Gamma(t), 0, 0]^T$$

$$[x_C(t), y_C(t), z_C(t)]^T = [C_0\Pi(t), 0, 0]^T$$

3D relative motion tracking: synchronous component moves along axis x, while asynchronous parts put to B moves along norm **n;**

$$[x_B(t), y_B(t), z_B(t)]^T = [\Gamma(t)n_x + C_1\Pi(t), \Gamma(t)n_y, \Gamma(t)n_z]^T$$

$$[x_C(t), y_C(t), z_C(t)]^T = [C_0\Pi(t), 0, 0]^T$$

All signals are sampled at 40 Hz and have a length of 1000 sampling points. Relative motion cancellation scheme is tested on a set of data contaminated by Gaussian noise $e_m(t)$ (with standard deviations varies from 0 to 0.5 with increment 0.01).

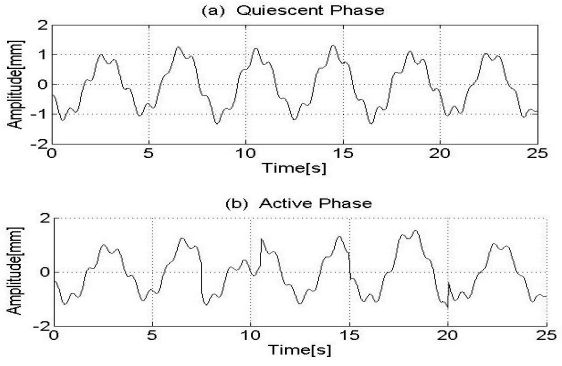

Fig. 3. Simulated data: (a) quiescent phase and, (b) active phase

As shown in Fig 4, 1D(a) and 3D (b) tracking absolute errors [mm] increases linearly with noise standard deviation growth, which indicates our relative motion tracking scheme are capable of motion compensation in a wide range of noise levels.

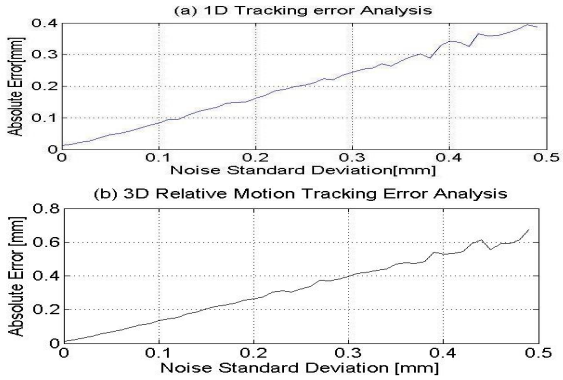

Fig. 4. Tracking error analysis

B. Phantom Experiment

To evaluate the supervised PDT scheme, we simulated the physiological movement on a silicon phantom of upper digestive tract, video collected on the phantom by endoscope was processed frame by frame to detect relative motion. ROI was defined in a square region, an ideal projected spot refers its minimum circumscribed circle. We experimented with respect to two general motion forms: absolute movement and relative movement.

Absolute movement experiment: endoscope located still, while phantom moved periodically and independently, the quiescent phase naturally corresponds to state without disturbance. As depicted in Fig 6, positions of ROI drift over time. Simulated motion tracking scheme was employed to stabilize virtual projected spot on ROI.

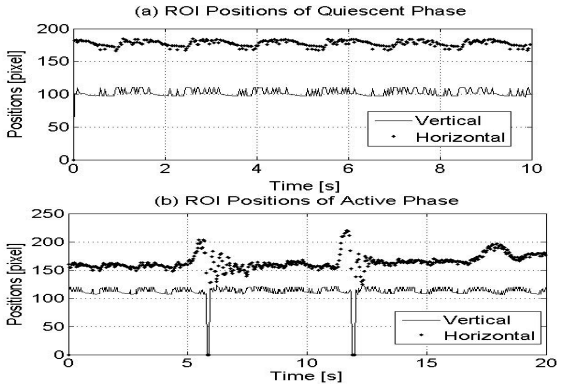

Fig. 5. ROI positions detected in absolute movement

By reference to the ideal circumstance that ROI tracked precisely, quantitative comparison in accumulative exposures to target lesion and healthy tissues of the supervised and unsupervised PDT respectively can be seen in Table 1. The supervised scheme outperforms over the unsupervised case, improvement in active phase is superior to that of quiescent state.

TABLE 1.
PERFORMANCE COMPARISON OF ABSOLUTE MOVEMENT

	Exposure to target lesions		Exposure to healthytissues	
	Unsupervised	Supervised	Unsupervised	Supervised
QP	61.50%	86.58%	167.55%	123.54%
AP	28.79	88.08%	224.93%	120.92%

QP:Quesient Phase; AP:Active Phase

Relative movement experiment: Regular pushes and irregular presses imposed on the phantom, endoscope moved cooperatively. The mixed movement video was collected and processed subsequently, relative motions between focused spot and ROI are shown in Fig 6.

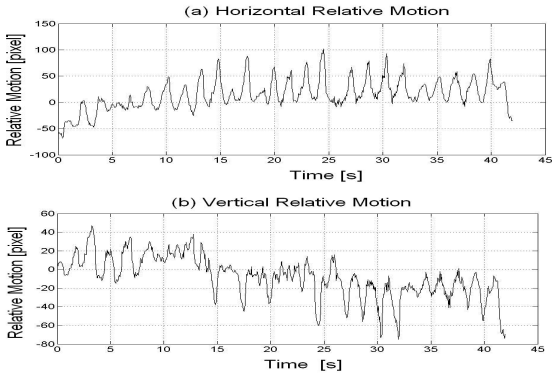

Fig. 6. Relative motion between focused spot and target ROI

Quantitative analysis of the relative movement was also concluded in Table 2, the result validates further the superiorities of the supervised over the unsupervised case.

TABLE 2.
PERFORMANCE COMPARISON OF RELATIVE MOVEMENT

	Exposure to target lesions		Exposure to healthytissues	
	Unsupervised	Supervised	Unsupervised	Supervised
MM	14.36%	94.91%	250.24%	108.94%

MM:Mixed Mode

IV. CONCLUSIONS

The supervised PDT scheme reported in this paper outperforms the unsupervised one both in speed and exposure to healthy tissue. Experiments on simulated data validate high efficiency of our relative motion tracking scheme, experiments on silicon phantom confirm these improvements. Therefore, the usage of light dose auto-evaluation and visual-servo strategy could benefit to endoscopically guided PDT. In the future we will develop a robotic-assisted PDT based on this principle.

REFERENCES

[1] THOMAS J. DOUGHERTY, An Update on Photodynamic Therapy Applications, Journal of Clinical LaserMedicine & Surgery, 0(1):3-7 , 2002

[2] K. Sharma, W. Newman, M. Weinhous, Experimental evaluation of a robotic image-directed radiation therapy system," in Proc. IEEE Int. Conf. Robot. Autom.,3:2913–2918 ,2000

[3] A. Schweikard, G. Glosser, M. Bodduluri, Robotic motion compensation for respiratory movement during radiosurgery, Comput. Aided Surg., 5(4):263–277 ,000

[4] Özkan Bebek, and M. Cenk Çavus¸o˘glu, Intelligent Control Algorithms for Robotic-Assisted Beating Heart Surgery, IEEE TRANS. ON ROBOTICS, 23(3):468-480,2007

[5] Giles W. Stevenson, Steven M. Collins, and Sat Somers, Radiological Appearance of Migrating Motor Complex of the Small Intestine. Gastrointest Radiology ,13:215-2189 ,1988 .

[6] Peter Mountney, Benny Lo, Surapa Thiemjarus, A Probabilistic Framework for Tracking Deformable Soft Tissue in Minimally Invasive Surgery, MICCAI 2007, Part II, LNCS 4792, 34–41,2007

[7] M. Baumhauer, M. Feuerstein, H.P. Meinzer, Navigation in Endoscopic Soft Tissue Surgery Perspectives and Limitations, JOURNAL OF ENDOUROLOGY, 22(4):751-766,2008.